Multi-energy soft-x-ray technique for impurity transport measurements in the fusion plasma edge

D J Clayton[1], K Tritz[1], D Stutman[1], M Finkenthal[1], S M Kaye[2], D Kumar[1], B P LeBlanc[2], S Paul[2] and S A Sabbagh[3]

[1] Department of Physics and Astronomy, The Johns Hopkins University, Baltimore, MD 21218, USA
[2] Princeton Plasma Physics Laboratory, Princeton, NJ 08543, USA
[3] Department of Applied Physics and Applied Mathematics, Columbia University, New York, NY 10027, USA

E-mail: dclayton@pppl.gov

Abstract

A new diagnostic technique was developed to produce high-resolution impurity transport measurements of the steep-gradient edge of fusion plasmas. Perturbative impurity transport measurements were performed for the first time in the NSTX plasma edge ($r/a \sim 0.6$ to the SOL) with short neon gas puffs, and the resulting line and continuum emission was measured with the new edge multi-energy soft-x-ray (ME-SXR) diagnostic. Neon transport is modeled with the radial impurity transport code STRAHL and the resulting x-ray emission is computed using the ADAS atomic database. The radial transport coefficient profiles $D(r)$ and $v(r)$, and the particle flux from the gas puff $\Phi(t)$, are the free parameters in this model and are varied to find the best fit to experimental x-ray emissivity measurements, with bolometry used to constrain the impurity source. Initial experiments were successful and results were consistent with previous measurements of core impurity transport and neoclassical transport calculations. New diagnostic tools will be implemented on NSTX-U to further improve these transport measurements.

(Some figures may appear in colour only in the online journal)

1. Introduction

An understanding of the leading causes of impurity and majority ion particle transport is of critical importance to the successful development of current and future spherical torus (ST) and tokamak devices [1, 2]. Direct measurements of the radial diffusive and convective transport coefficient profiles, $D(r)$ and $v(r)$, coupled with plasma turbulence measurements, can shed light on the nature of deviations from neoclassical theory. To properly determine both $D(r)$ and $v(r)$ independently, perturbative transport measurements should be employed [1, 2]. To this end, impurity transport has been measured in the National Spherical Torus Experiment (NSTX) [3] using short puffs of non-intrinsic impurity gases such as neon [4–6]. While impurity transport is commonly measured in the core plasma of toroidal fusion devices (see [1, 2] and the references therein), there are added complications

when measuring impurity transport toward the plasma edge. Sources of neutral particles at the plasma boundary, such as from wall recycling, must be accounted for. Sharp temperature gradients in the edge pedestal region of tokamaks and STs necessitate diagnostics with high spatial resolution, as well as create large gradients in ionization state distributions, which limits the usefulness of diagnostics that rely on line emission from a single charge state. A practical solution to this problem is to use photodiode-based diagnostics that measure broadband emission, as has been previously carried out on some conventional tokamaks [7, 8]. On NSTX, a new diode-based diagnostic, utilizing multiple filters to help distinguish low-charge-state emission from higher charge state emission, has been used to measure impurity transport in the ST plasma edge for the first time. Emission from low-charge states, measured with thinner filters, provides the source terms for transport analyses of higher charge states. For this type of

diagnostic, proper modeling of all types of continuum and line emission becomes important. In addition to the effects of turbulence, the effects of 3D magnetic field perturbations on impurity particle transport in the plasma edge are of particular interest as scientists attempt to understand the relationship between these perturbations and ELM suppression [9].

2. Multi-energy SXR diagnostic

To address the challenge of measuring electron thermal and impurity particle transport within a wide range of plasma temperatures, multi-energy soft-x-ray (ME-SXR) diagnostics have been developed [10–13]. These instruments provide SXR emissivity measurements with coarse spectral resolution and fine spatial and time resolution. For the NSTX plasma edge, a system of five 20-channel silicon photodiode arrays, each with a view of essentially the same plasma volume, was constructed and implemented [13]. Four arrays have different foil filters (currently 0.3 μm Ti, 5 μm Be, 15 μm Be and 50 μm Be) to provide 4-color spectral resolution, and the fifth array, with no filter, is used for bolometry. The filters discriminate line

emission from groups of impurity ionization states as seen in figure 1. For measurements of neon puffed into the plasma edge, the bolometer signal is dominated by L-shell emission, while the 5 μm Be filter picks up primarily K-shell lines (H-like and He-like neon). The 50 μm Be array measures continuum emission from fully stripped neon. The Ti filter was chosen specifically to measure C V and C VI emission; for the case of neon, the response of the 0.3 μm Ti filtered array is similar to the 5 μm Be array. Each array has a mid-plane tangential view of the plasma edge with radial coverage from $r/a \sim 0.6$ to the scrape-off layer (SOL), with a radial resolution of 1 cm. Variable-gain preamplifiers produce a signal with high time resolution, ranging from about 10 kHz for high gain to greater than 100 kHz for low gain. Second-stage amplifiers are used to further boost the signal for digitization. In conjunction with other impurity-monitoring spectrometers, such as the transmission-grating based imaging spectrometer (TGIS) [14], the ME-SXR arrays can provide fast T_e and impurity density measurements for transport calculations. A description of the technique now being implemented to quantify impurity transport in the plasma edge follows.
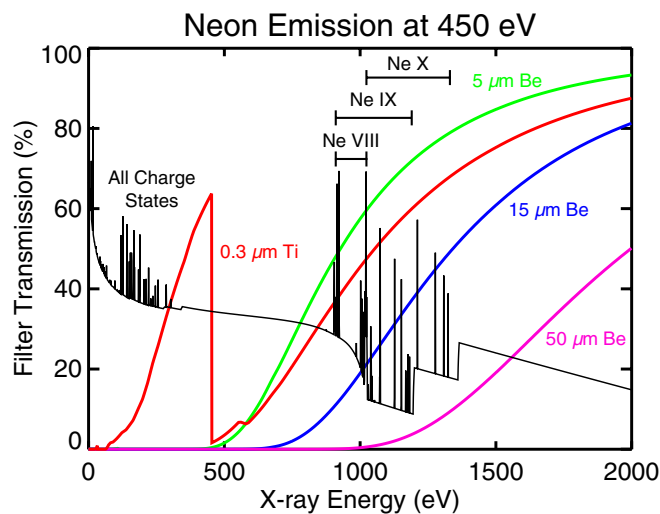
3. Impurity transport analysis

3.1. Impurity transport and x-ray emission modeling

To model the particle transport of an injected impurity, we use the STRAHL 1D impurity ion radial transport code [15]. For a given impurity, the density evolution of each ionization state is described by a transport equation with a flux-surface averaged diffusion coefficient $D(r, t)$ and convective velocity $v(r, t)$ provided by the user. The particle source/sink term for each ionization state depends on n_e, T_e, and the density of neighboring states through the rate coefficients for ionization and the recombination coefficients for radiative and dielectronic recombination. Neutral deuterium density is not diagnosed in NSTX and is assumed to be negligible inside the separatrix, thus recombination coefficients due to charge exchange are not included in the model. All rate coefficients, along with x-ray emissivity coefficients, are obtained from the ADAS atomic database [16]. The plasma parameters n_e
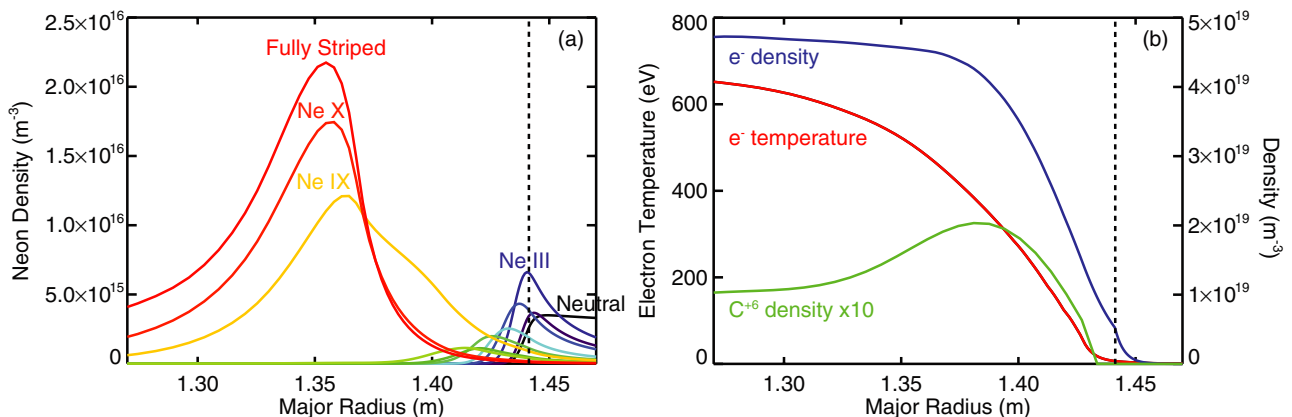

Figure 1. The x-ray transmission of the beryllium foils over-plotted on the spectrum emitted by neon in a 450 eV plasma (on a log scale).

Figure 2. (*a*) Typical distribution of neon ionization states in NSTX 20 ms after a neon injection at the plasma edge, in this case from the $I_p = 1.1$ MA, $B_T = 0.55$ T discharge described in the following section. (*b*) Electron temperature and density, measured with Thomson scattering, and C^{6+} density, measured with charge exchange recombination spectroscopy, from this discharge at this time.
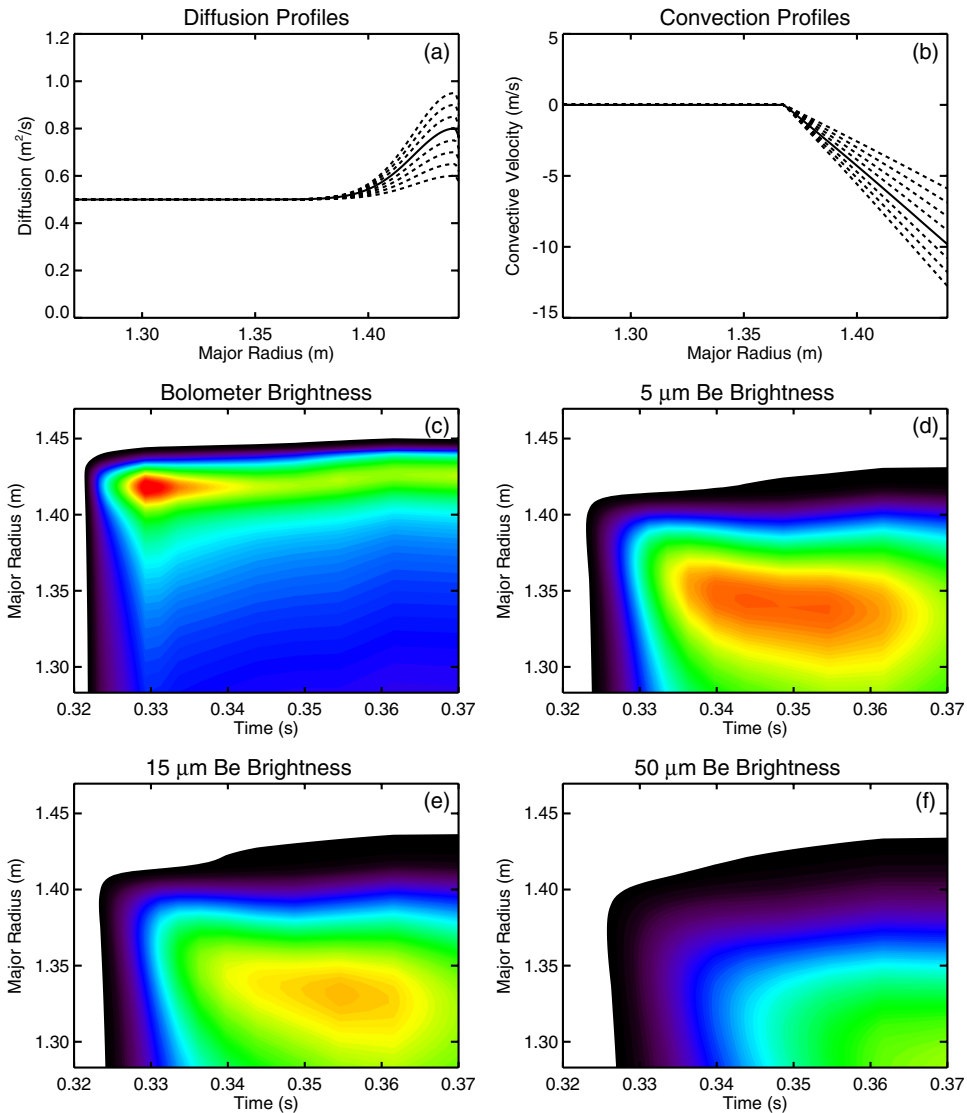
Figure 3. (*a*)–(*b*) Transport coefficient profiles used to generate simulated ME-SXR data (solid lines) and the profiles used to fit this simulated data (dashed lines). (*c*)–(*f*) Simulated ME-SXR data for the bolometer array and the three beryllium-filtered arrays.

and T_e are measured with Thomson scattering. Along with D and v, the third free parameter in this transport model is the source of neutral impurity atoms, both directly from the impurity injection and from divertor and vacuum vessel wall recycling.

STRAHL's radial grid is defined from the core to the boundary and includes the SOL. Neutral particles are introduced at the wall, defined to be 10 cm from the separatrix, with a user-defined flux. These particles are at room temperature and move into the plasma with the appropriate thermal velocities until they are ionized in the SOL or inside the separatrix. Ions in the SOL are transported radially, as they are inside the separatrix, but may also be lost to the divertor with a user-defined connection length (10 m was used for NSTX) and impurity Mach number (0.5 was used for NSTX). Particles transported outward may be lost to the wall before reaching the divertor. An impurity recycling coefficient, also supplied by the user, is applied to the wall, allowing for lost particles to re-enter the grid as room-temperature neutrals. For the case of neon in NSTX, a recycling coefficient of 0.95 best fits the

data. The NSTX divertor does not have active pumping, and particles lost to the divertor return to the SOL with a user-defined characteristic time of about 1 ms.

A simple synthetic diagnostic uses the densities of each charge state of an impurity, calculated by STRAHL, to determine the filtered x-ray intensities that would be measured by the ME-SXR system. A typical neon charge state distribution found with STRAHL is shown in figure 2(*a*), revealing that only the highest charge states are found inside the NSTX pedestal. For reference, electron temperature and density and the density of fully ionized carbon, the predominant intrinsic impurity in NSTX discharges, are plotted in figure 2(*b*). ADAS routines are used to calculate the free–free and free–bound continuum emission and the photon emissivity coefficients for line emission from electron impact excitation and from radiative and dielectronic recombination. This total emission is then integrated along the line of sight of each detector and normalized by the transmission of the filter, the detector response and detector etendue.
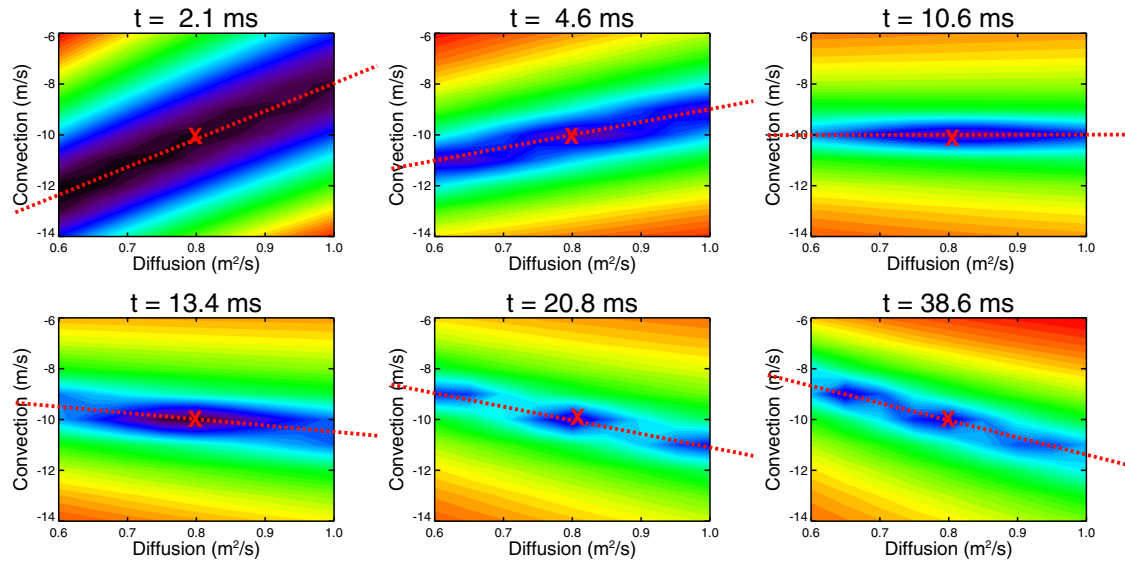
Figure 4. Chi square of model's fit to simulated data versus $D(r/a = 1)$ and $v(r/a = 1)$ for 6 time points. The Xs mark the correct solution, used to generate the simulated data. The dashed lines highlight the set of D and v values that best match the simulated data at that time. The line rotates about the correct values as time evolves.

3.2. Fitting the model to experimental data

To solve for the transport coefficient profiles, this model is fit to the measured data by applying a chi square minimization, with the radial D and v profiles and the neutral source term acting as the free parameters. Note that on the time scale of the gas-puff perturbation ($\sim$20 ms), the D and v profiles are assumed to be constant in time, thus experimental plasma conditions are chosen to avoid transients such as ELMs. STRAHL assumes a static magnetic equilibrium while experimentally, the magnetic flux surfaces, including the separatrix, shift radially in time. To account for this, STRAHL's input parameters are mapped to a normalized poloidal flux coordinate ρ_{pol} using the MHD equilibrium code EFIT [17], and the resulting x-ray emission is mapped back to major radius. For this work, $D(r)$ and $v(r)$ are defined using linear interpolations between knots at $\rho_{pol} = \{0.6, 0.7, 0.8, 0.9, 1.0\}$. SOL transport is set equal to the values of the knot at $\rho_{pol} = 1.0$. A core SXR measurement was not available when these measurements were performed, and the edge measurements are insufficient to constrain transport inside $r/a \sim 0.6$. Therefore, based on previous core measurements demonstrating neon transport to be neoclassical in the core of NSTX discharges under nearly identical conditions [5, 6], $D(r)$ and $v(r)$ are fixed to neoclassical values for $\rho_{pol} \leqslant 0.5$, with a linear interpolation between $\rho_{pol} = 0.5$ and the knot at $\rho_{pol} = 0.6$.

The neoclassical $D(r)$ and $v(r)$ profiles were calculated using the NCLASS code [18]. Ion–ion collisions with deuterium and with carbon, the main impurity species, were included. Carbon density and temperature profiles were measured with a charge-exchange recombination spectroscopy diagnostic. Although lithium wall conditioning was performed for these experiments, spectroscopy has shown that very little lithium enters the plasma and it is thus left out of the calculations [19]. Neoclassical neon transport falls in the Pfirsch–Schlüter regime throughout the plasma volume for all cases considered due to its high collisionality, particularly with carbon.

To study the sensitivity of this procedure to diffusion versus convection at the plasma edge, simulated data were generated by running STRAHL with the simplified transport coefficient profiles shown in figures 3(*a*) and (*b*) (solid lines) and adding Gaussian noise to the signal at a level comparable to the noise in the experimental ME-SXR signals. The results are shown in figures 3(*c*)–(*f*) and closely resemble actual experimental measurements. The edge diffusion and convection profiles used by the model were then varied as shown with the dashed lines in figures 3(*a*) and (*b*). In each case, the chi square of the fit of the model to the simulated data was computed. An initial attempt to fit the simulated 2D (radial and time) profiles throughout the entire duration of the perturbation did not converge to a unique D and v solution. The fits were dominated by the later stages of the gas-puff perturbation, when the impurity profiles approach a steady state. In a steady state, only the D/v ratio can be found. To rectify this problem, the chi square minimization can be performed on only the first 2 ms of the perturbation, when the impurity profiles are quickly evolving. The contour plots in figure 4 show these resulting chi square values versus D and v for various time points following the gas puff. These figures reveal that for one time point, D and v cannot be independently determined. A dashed line highlights the set of possible solutions. However, as time evolves this line rotates about a fixed pivot, marked with an X, which represents the unique solution. Note that the line stops rotating after $\sim$20 ms, and time resolution on the order of 1 ms is required to perform this measurement.

For the case of neon injection, the higher charge states (Ne IX, Ne X, Ne XI) dominate the charge state distribution in a hot fusion plasma such as in NSTX, and these are the charge states that are primarily used for impurity transport measurements. However, monitoring the lower charge states
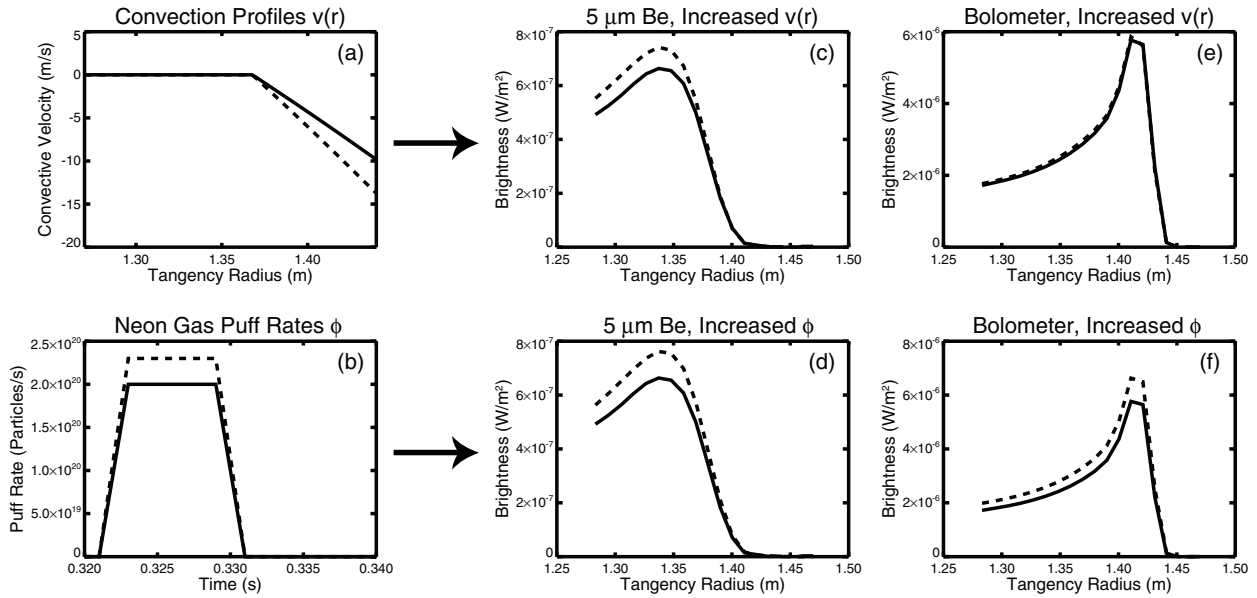
Figure 5. Increases in (*a*) the inward convection and (*b*) the gas-puff flow rate appear to have the same effect on (*c*)–(*d*) the 5 μm Be filtered brightness, shown here 50 ms after the start of the gas puff. However, the effects on (*e*)–(*f*) the bolometry signal 50 ms after the puff are quite distinct.

of neon is equally important, as these ions act as the source, through ionization, of the higher charge states. Emission from these low-charge states is primarily below even the 5 μm beryllium foil's cutoff energy, and must instead be measured with bolometry. The importance of the bolometer, which places a constraint on the source term of the higher charge states measured with the filtered arrays, is demonstrated in figure 5. An increased gas-puff injection flux can have the same effect on filtered x-ray emission profiles as an increased inward convection of low-charge-state particles, but these two effects are quite distinct when measured with bolometry. The effects of transport and impurity source on x-ray emissivity are coupled; the source must be known to determine the transport coefficients.

When the model is fit to actual ME-SXR data, a chi square minimization is performed with MPFIT [20], a Levenberg–Marquardt non-linear least squares fitting routine, with the radial D and v profiles and the time-dependent neutral source term as free parameters. Background emission from intrinsic impurities, measured before neon gas injection or in discharges without injection, is found to be small and slowly varying on the timescales of the gas-puff perturbation ($\sim$20 ms). For the purposes of this analysis, the emission at the start time of the gas puff is subtracted from the measurement and the remaining signal is assumed to be solely due to neon emission. For the initial perturbative impurity transport measurements described in the next section, the ME-SXR diagnostic was not yet fully constructed; only the 5 μm Be array and fractions of the 15 μm and 50 μm Be arrays were available. In place of the ME-SXR edge bolometer array, a separate bolometer, with a coarser spatial resolution covering the entire plasma radius, was employed to constrain the source term. Using for an example the high-field case described in the following section, figure 6 shows good agreement between the radiated power measured with the bolometer and computed from the best-fit
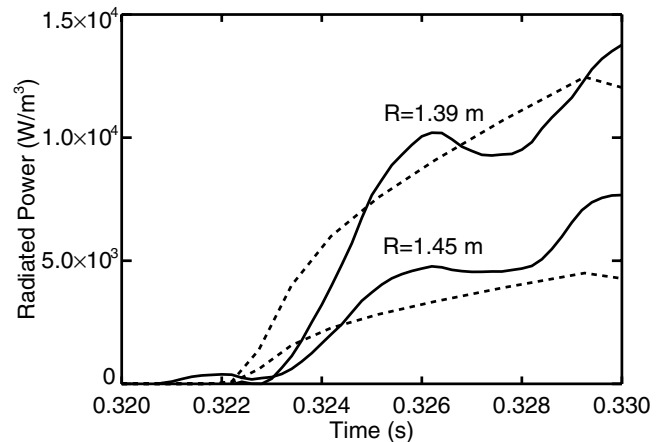

Figure 6. Time evolution of the total radiated power, measured by the core bolometer (solid lines) for the two lines of sight through the plasma volume also covered by the ME-SXR edge diagnostic, and radiated power computed from the best-fit model (dashed line) for the $I_p = 1.1$ MA, $B_T = 0.55$ T case described in the next section.

model. While the additional filtered arrays are required for the temperature modeling for which the diagnostic was primarily designed, the limited diagnostic, together with the bolometer, is sufficient for impurity transport measurements within a limited plasma volume of the appropriate temperature. Use of the additional arrays would provide measurements of emission from other charge states, allowing for transport measurements across the entire plasma volume and reducing uncertainty in the source/sink terms between the ionizations states.

4. Initial experimental results and discussion

Perturbative impurity transport measurements were performed in NSTX using short 5 ms neon gas puffs at the outboard mid-plane, injecting about 2.5×10^{17} neon particles. Electrons
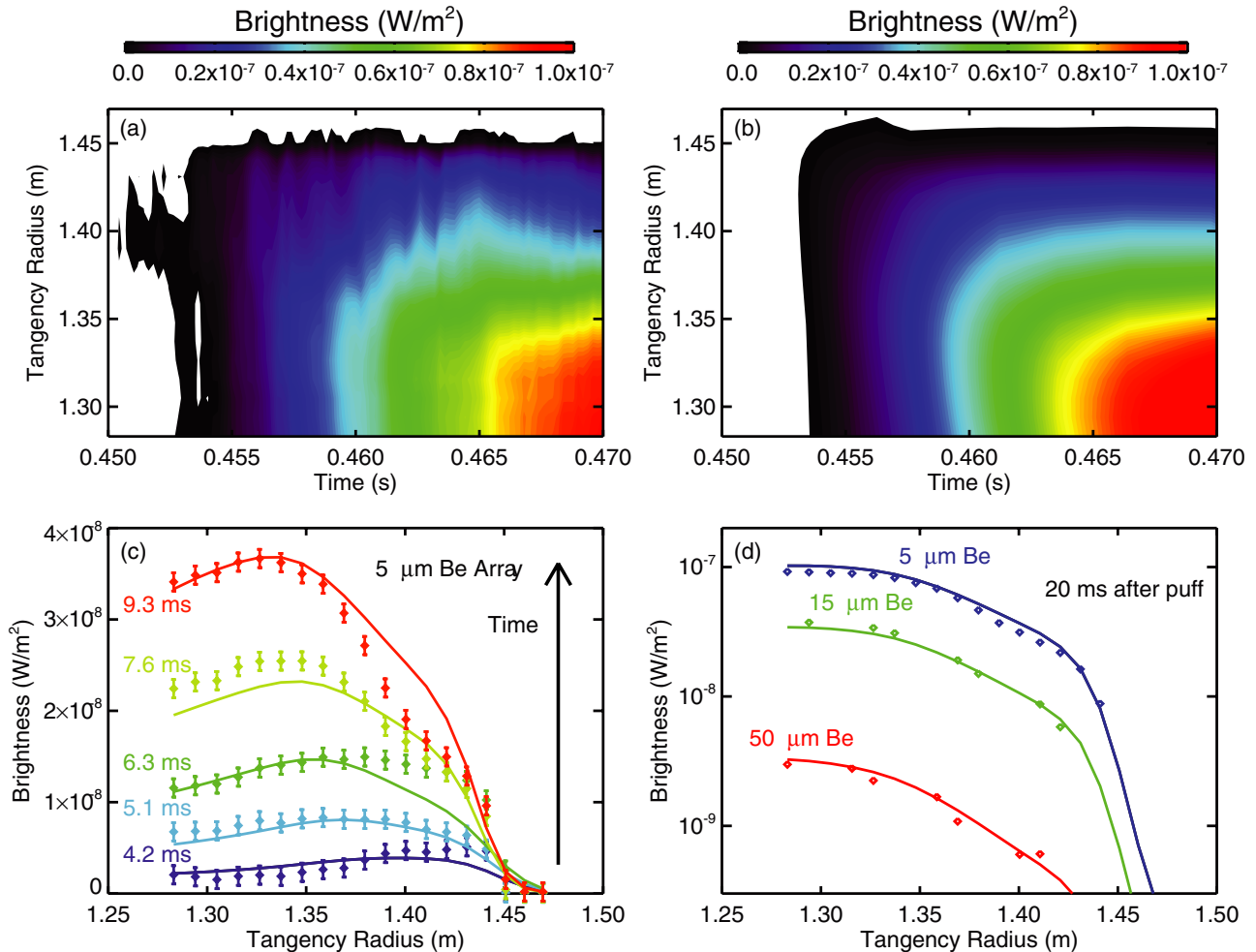
Figure 7. (*a*) Contours of time-evolving x-ray brightness profiles from the $I_p = 0.8$ MA, $B_T = 0.40$ T discharge, measured with the 5 μm Be array. (*b*) Modeled brightness that best fits the data in (*a*). (*c*) Five time slices from (*a*)–(*b*), showing the evolution of the brightness profile shortly after the gas puff. (*d*) A time slice of the brightness profiles from the 5 μm Be array compared with the 15 μm and 50 μm Be arrays. The points represent measurements and the solid lines represent the fits from the model.

from the neon puff accounted for only about 0.5% of the total plasma electron density, and Thomson scattering indicates that the perturbation to the bulk plasma was negligible. A toroidal field scan was performed, with q_{95} kept roughly constant by scaling the plasma current accordingly: 0.8 MA at 0.40 T, 0.9 MA at 0.45 T and 1.1 MA at 0.55 T. Additionally, a few high-current (1.1 MA), low-field (0.45 T) discharges were obtained. MHD-quiescent, ELM-free discharges were desired to prevent large changes in the measured transport quantities on the time scales of the neon perturbation, a few tens of ms. To this end, the neutral beam power was stepped down from 6 to 4 MW after current ramp-up to reduce fast-ion driven modes. Lithium wall conditioning was utilized in an effort to reduce ELM activity. In addition to the ME-SXR array, key diagnostics for the experiment included Thomson scattering for electron temperature and density profile measurements, and magnetic diagnostics, including MSE, needed for equilibrium reconstructions with EFIT.

ME-SXR brightness measurements from an $I_p = 0.8$ MA, $B_T = 0.40$ T discharge, along with fits from the transport model, are shown in figure 7. The impurity transport profiles resulting from this fit, and from a fit of an $I_p = 1.1$ MA and

$B_T = 0.55$ T discharge, are shown in figure 8. The error bars represent the uncertainty in the transport profiles due to uncertainty in the ME-SXR and Thomson measurements and in the neoclassical values used to constrain core transport. There are additional sources of error, described below, that are not included in these error bars. For comparison, the results from the NCLASS neoclassical transport calculations are shown with shaded regions on the plots, covering the variation in the calculations during the time frame of the measurement. While the plasma parameters evolve slightly during the time frame of the transport measurement, the variation in the NCLASS results is due primarily to uncertainties in the gradients of edge temperature and density measurements. The results from the measurements roughly match neoclassical calculations, in agreement with previous results from the core [5, 6]. The diffusion coefficients obtained from measurements are within a factor of 2 of neoclassical transport across most of the plasma radius. Deviations from neoclassical diffusion in the edge region, particularly in the far edge of the low-field discharge, are likely due to edge turbulence and are the topic of ongoing studies. The convection profiles also roughly agree with neoclassical values, though NCLASS does not
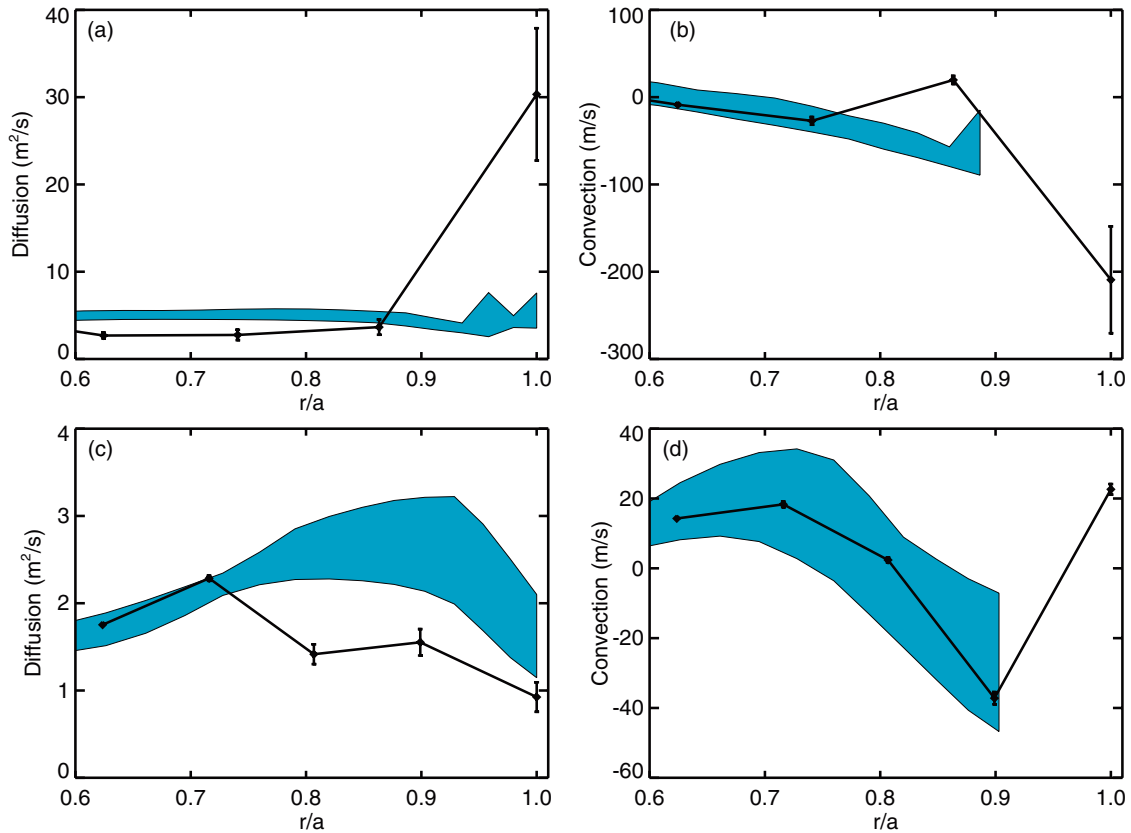
Figure 8. (*a*) The resulting diffusion profile and (*b*) convection profile from the $I_p = 0.8$ MA, $B_T = 0.40$ T discharge. The shaded region represents the results from NCLASS neoclassical transport calculations. (*c*) Diffusion profile and (*c*) convection profile for the $I_p = 1.1$ MA, $B_T = 0.55$ T case. The radial knots are defined for fixed values of ρ_{pol} and thus shift radially between the two cases with different q profiles.

provide reliable convective velocities outside of $r/a \sim 0.9$. For the two cases shown, the neoclassical convective velocity remains outward far into the core, which is consistent with the hollow neon profile found in the STRAHL simulations at later times. Previous results from core measurements have shown that neon convection near mid-radius can be either inward or outward, depending on the ion temperature and density profiles, and that neon profiles can thus be either peaked or hollow [5, 6]. In conclusion, inside the pedestal region and under the conditions of these quiescent discharges, plasma turbulence is not sufficient to alter transport from neoclassical levels.

Several factors currently limit the spatial resolution of these transport measurements and can contribute additional uncertainty. One factor affecting both the uncertainty and resolution is the presence of edge fluctuations. Although precautions were taken to avoid large fluctuations, some small fluctuations still remained; for instance, small ~ 1 kHz fluctuations can be seen in figure 7(*a*). With the assumption that transport remains roughly constant through the duration of the perturbation, the fit in figure 7(*b*) averages over these fluctuations. Another factor contributing to the uncertainty in the results is the lack of an emissivity measurement inside $r/a \sim 0.6$. Transport inside this radius is essentially unconstrained. As discussed in previous sections, for the current work, transport is assumed to be neoclassical in the core, though in less quiescent plasmas this may not be the case.

Other reasons for increased uncertainty are due to unknowns in the neutral source term when using neon gas. The time evolution of the gas injection from the puffer is unknown, as it was not designed for such short puffs. Also, neon is a recycling impurity, with impurity ions lost to the wall reentering the plasma at an unknown rate. For the NSTX experiments described above, it was assumed that the unknown gas-puff time evolution profile and neon recycling rates were the same in each discharge, and the values were found that best fit all cases. Finally, without the bolometer array, high-resolution measurements of the pedestal region (outside of $r/a \sim 0.9$) were not possible, allowing only for an average value for the region.

To address some of these issues, new diagnostic tools will be implemented on the upcoming NSTX-Upgrade (NSTX-U). The first improvement will be the construction a diagnostic with two sub-arrays: an edge sub-array, similar in design to the current diagnostic, and a core sub-array, which will view the entire plasma volume with coarser spatial resolution. In addition to providing a core transport measurement, the core sub-array will provide an inner boundary condition when fitting edge measurements. The second new diagnostic tool will be a laser blow-off system that will inject non-recycling impurities into the plasma for perturbative impurity (and heat) transport measurements. One advantage of laser blow-off over gas puffs is the quick, precise injection of the impurities. The gas-puff valves in NSTX take 2–3 ms simply to open or

close; by contrast, a laser ablation system delivers impurities on a time scale of ∼1 ms. Additionally, while neutrals from gas puffs are at room temperature and can take several milliseconds to traverse the distance between the gas-puff valve and the plasma separatrix, ablated neutrals have energies on the order of an eV and travel from the ablated substrate to the separatrix within a negligible time. The time history of a laser blow-off injection can be monitored via neutral emission, measured with a filtered diode. This time history places an additional constraint on the STRAHL model and thus reduces the resulting uncertainty in the transport coefficient profiles. Finally, laser blow-off can be used to inject non-recycling impurities, versus the highly recycling gases typically available for puffing. The use of non-recycling impurities will eliminate the need to include recycling in the STRAHL model, which will further reduce the uncertainty. Another major advantage of non-recycling impurities is that they will allow for multiple transport measurements during a single discharge. Lastly, it should be pointed out that laser ablation will provide the injection of impurities relevant to fusion devices, particularly materials used for plasma-facing components (C, Mo, W, etc).

5. Conclusions

Initial tests of the new multi-energy SXR diagnostic have shown the system to be capable of measuring fast x-ray emissivity perturbations from a neon gas injection, and from this impurity transport profiles have been inferred. Radial impurity transport modeling with the STRAHL code and emissivity calculations utilizing the ADAS atomic database have successfully reproduced experimental measurements with the ME-SXR array. The diffusion and convection profiles that produce the best fits to the data closely match earlier measurements with a core ME-SXR array, but with improved resolution. The profiles are roughly neoclassical, though at least in the low-field case, the diffusion appears anomalous in the pedestal region.

Experiments will be proposed to measure edge impurity transport under a variety of plasma conditions in NSTX-U, including a study of the effects of applied 3D fields on impurity transport. Multiple impurity species will be used to obtain Z scalings in each case. These diagnostic tools will be used together with turbulence diagnostics to search for causes of any measured anomalous transport in these new, high-performance ST plasmas.

References

[1] Lopes Cardozo N J 1995 *Plasma Phys. Control. Fusion* **37** 799
[2] Ryter F, Dux R, Mantica P and Tala T 2010 *Plasma Phys. Control. Fusion* **52** 124043
[3] Ono M *et al* and NSTX team 2000 *Nucl. Fusion* **40** 557
[4] Stutman D, Finkenthal M, Bell R E, Kaye S M, LeBlanc B P, Menard J E, Synakowski E J, Darrow D S, Bourdelle C and The NSTX Team 2003 *Phys. Plasmas* **10** 4387
[5] Delgado-Aparicio L *et al* 2009 *Nucl. Fusion* **49** 085028
[6] Delgado-Aparicio L *et al* 2011 *Nucl. Fusion* **51** 083047
[7] Dux R 2003 *Fusion Sci. Technol.* **44** 708
[8] Sunn Pedersen T, Granetz R S, Hubbard A E, Hutchinson I H, Marmar E S, Rice J E and Terry J 2000 *Nucl. Fusion* **40** 1795
[9] Zeng L, Doyle E J, Rhodes T L, Schmitz L, Peebles W A, Evans T E, Mordijck S, Moyer R A, McKee G R and Yan Z 2011 *Bull. Am. Phys. Soc.* **56** 97
[10] Delgado-Aparicio L F, Stutman D, Tritz K, Finkenthal M, Kaita R, Roquemore L, Johnson D and Majeski R 2004 *Rev. Sci. Instrum.* **75** 4020
[11] Delgado-Aparicio L F *et al* 2007 *Plasma Phys. Control. Fusion* **49** 1245
[12] Tritz K, Stutman D, Delgado-Aparicio L, Finkenthal M, Kaita R and Roquemore L 2010 *Rev. Sci. Instrum.* **81** 10E502
[13] Tritz K, Clayton D J, Stutman D and Finkenthal M 2012 *Rev. Sci. Instrum.* **83** 10E109
[14] Kumar D, Finkenthal M, Stutman D, Bell R E, Clayton D J, Diallo A, LeBlanc B P, Podesta M and Tritz K 2012 *Plasma Phys. Control. Fusion* **54** 065010
[15] Behringer K 1987 Description of impurity code 'STRAHL', *Technical Report* JET-IR(87)08, JET Joint Undertaking, Oxfordshire, Abingdon
[16] Summers H P 1994 Atomic Data and Analysis Structure *Technical Report JET*-IR(94)06, JET Joint Undertaking, Oxfordshire, Abingdon
[17] Sabbagh S A *et al* and NSTX Research Team 2001 *Nucl. Fusion* **41** 1601
[18] Houlberg W A, Shaing K C, Hirshman S P and Zarnstorff M C 1997 *Phys. Plasmas* **4** 3230
[19] Podestà M, Bell R E, Diallo A, LeBlanc B P, Scotti F and The NSTX Team 2012 *Nucl. Fusion* **52** 033008
[20] Markwardt C B 2008 *Proc. Astronomical Data Analysis Software and Systems XVIII* (*ASP Conference Series* vol 411) ed D Bohlender *et al* (San Francisco, CA: Astronomical Society of the Pacific) pp 251–4